Multipolar blackbody radiation shifts for single-ion clocks

Bindiya Arora,[1] D. K. Nandy,[2] and B. K. Sahoo[2,*]
[1]*IISER Mohali, Sector 81 Mohali, Manouli 140306, India*
[2]*Theoretical Physics Division, Physical Research Laboratory, Ahmedabad 380009, India*
(Received 8 August 2011; revised manuscript received 12 December 2011; published 4 January 2012)

Appraising the projected 10^{-18} fractional uncertainty in the optical frequency standards using singly ionized ions, we estimate the blackbody radiation (BBR) shifts due to the magnetic dipole ($M1$) and electric quadrupole ($E2$) multipoles of the applied external electromagnetic field. Multipolar scalar polarizabilities are determined for the singly ionized calcium (Ca^+) and strontium (Sr^+) ions using the relativistic coupled-cluster method, though the theory can be exercised for any single-ion clocks. The expected energy shifts for the respective clock transitions are estimated to be $4.38(3) \times 10^{-4}$ Hz for Ca^+ and $9.50(7) \times 10^{-5}$ Hz for Sr^+. These shifts are large enough and may be a prerequisite for the frequency standards to achieve the foreseen 10^{-18} precision goal.

DOI: 10.1103/PhysRevA.85.012506 PACS number(s): 31.15.bw, 32.10.Dk, 06.30.Ft, 32.80.−t

I. INTRODUCTION

Optical transitions with ultranarrow frequencies in the single positively charged ions that use advanced laser cooling and trapping techniques are of current interest for frequency standards [1–3]. Some of the successful single-ion optical atomic clocks are Hg^+ [4,5], Ca^+ [6], Sr^+ [7,8], Al^+ [3,9], Yb^+ [10], and so on, and among these the fractional uncertainty in Hg^+ and Al^+ has already reached 10^{-17} [3]. A new range of experiments are also proposed for other ions like Ba^+ [11,12], Ra^+ [13,14], In^+ [15,16], and Yb^+ [17]. More precise frequency standards will open up possibilities to study the underlying physics related to fundamental constants, probing new elementary physics, and, more importantly, it can help in improving the present-day global positioning systems and also in tracking deep-space probes [1,5,18–20].

One of the major fortifications to attain smaller fractional uncertainties in the optical frequency standard measurements using ions is the accurate estimation of blackbody radiation (BBR) shifts. The considered standard frequency is shifted from the atomic resonance value due to the interaction of the ion with the external stray electromagnetic fields present in and around the experimental apparatus [21]. The BBR shift is caused by the isotropic field radiated due to finite temperature of the apparatus [21–23].

The dominant contribution to the BBR-induced energy shift is from the electric dipole ($E1$) component of the radiation field, which has been gauged by many groups for a number of ions using the relativistic theories [13,24–29]. However, there is absolutely no rigorous estimate of the BBR shifts due to higher multipoles for any proposed scheme. Following the derivations for the $E1$ BBR shift in Refs. [21–23], Porsev and Derevianko have given a generalized derivation [26] to deduce the BBR shifts spawned by any multipole component of the electromagnetic field. In their work, formulas for polarizability in the general case were also presented.

Two of the proficiency gadgets for the optical frequency standards are with a single calcium ion ($^{43}Ca^+$) [30,31] trapped in a Paul trap and with a strontium ion ($^{88}Sr^+$) confined in an endcap trap [7,32]. The considered clock transitions in these ions are the $s_{1/2} \rightarrow d_{5/2}$ transitions operating in the optical regime; the principles are also similar to the proposed Ba^+- [11,12], Ra^+- [13,14], and Yb^+-based [10,17] frequency standards. A major advantage of using the $^{43}Ca^+$ ion is that the radiation required for cooling, repumping, and clock transition is easily produced by a nonbulky solid state or diode laser [30]. The reported frequency measurements of the transition for frequency standard in $^{88}Sr^+$ have achieved a spectral resolution of better than 1.5 Hz [7,32–34]. As has been proclaimed, these experiments have the dexterity to diminish the relative systematic uncertainties to a level of 10^{-17} or below [7,13,14]. In such a scenario, it is compelling to estimate the BBR shifts caused by the higher multipoles, especially through the $M1$ and $E2$ channels for the experiments comprising the $s_{1/2} \rightarrow d_{5/2}$ transitions as in the above ions. Such an attempt was made by Porsev and Derevianko [26] for divalent atoms like Mg, Ca, Sr, and Yb. In this paper, we extend the work to preview the BBR shifts commenced by the $M1$ and $E2$ multipoles in the ions and in particular for the $^{43}Ca^+$ and $^{88}Sr^+$ ions where efficacious experiments are in progress to reduce the uncertainties over their previous measurements [6,7,30,32–34].

The paper is organized as follows. First, we discuss the inception of the BBR shifts which embody the $M1$ and $E2$ contributions of the radiation field. We then discuss the method of calculation in the $^{43}Ca^+$ and $^{88}Sr^+$ ions, subsequently presenting the results for the above multipolar contributions to the BBR shifts in these ions before summarizing the work. Unless stated otherwise, we use the conventional system of atomic units (a.u.), in which e, m_e, $4\pi\epsilon_0$, and the reduced Planck constant $\hbar$ have the numerical value 1.

II. THEORY

The interaction Hamiltonian between an electron in an atomic system with the external propagating electromagnetic field in the Coulomb gauge coupling is given by

$$\begin{aligned} V(r,\omega) &= -c\,\boldsymbol{\alpha}\cdot\mathbf{A}(r,\omega) \\ &= -c\,(\boldsymbol{\alpha}\cdot\hat{\boldsymbol{\epsilon}})\,\exp(i\mathbf{k}\cdot\mathbf{r}), \end{aligned} \tag{1}$$

where $\boldsymbol{\alpha}$ is the Dirac matrix in operator form, ω is the angular frequency of the field, and $\mathbf{k} = k\hat{k}$ and $\hat{\boldsymbol{\epsilon}}$ are its wave vector and polarization direction, respectively. In the presence of

*bijaya@prl.res.in

this interaction, the energy shift that can occur for an atomic energy level $|\Psi_n\rangle$ with energy $E_n = \omega_n$ can be approximated to Refs. [22,23],

$$\delta E_n(\omega) = \frac{1}{2}\sum_{m\neq n} |V_{nm}(r,\omega)|^2 \left[\frac{\omega_n - \omega_m}{(\omega_n-\omega_m)^2 - \omega^2}\right]. \quad (2)$$

Using the multipolar expansion and in terms of the traditional multipole moments $Q^{\lambda}_{LM}(\mathbf{k}\cdot\mathbf{r})$, we have [35]

$$\begin{aligned}(\boldsymbol{\alpha}\cdot\hat{\boldsymbol{\epsilon}})\ \exp(i\mathbf{k}\cdot\mathbf{r}) &= -\sum_{LM}\frac{(k^L)(i^{L+1+\lambda})}{(2L+1)!!}\left[\mathbf{Y}^{\lambda}_{LM}(\hat{k})\cdot\hat{\boldsymbol{\epsilon}}\right]\\ &\quad\sqrt{\frac{4\pi(2L+1)(L+1)}{L}}Q^{\lambda}_{LM}(\mathbf{k}\cdot\mathbf{r}),\\ &= -\sum_{LM,l}\frac{(k^L)(i^{L+1+\lambda})}{(2L+1)!!}Y^{\lambda}_{LM}(k_l)\\ &\quad\sqrt{\frac{4\pi(2L+1)(L+1)}{L}}Q^{\lambda}_{LM}(r_l), \quad (3)\end{aligned}$$

where k_l is the component of $\mathbf{k}$ projecting toward the l^{th} unit vector of $\hat{\boldsymbol{\epsilon}}$ and $\lambda = 1$ and $\lambda = 0$ correspond to the electric and magnetic multipoles, respectively.

Since the blackbody radiation is isotropic, each component of the electric and magnetic fields is related to the spectral energy density as

$$\begin{aligned}u(\omega,T) &= \frac{3}{8\pi}E_l^2(\omega) = \frac{3}{8\pi}B_l^2(\omega)\\ &= \frac{1}{\pi^2c^3}\frac{\omega^3}{\exp(\omega/k_BT)-1}, \quad (4)\end{aligned}$$

$\mathbf{B} = \boldsymbol{\nabla}\times\mathbf{A}$ and $\mathbf{E} = \frac{i\omega}{c}\mathbf{A}$, the energy shift after averaging over ω for all the polarization and propagation directions is given as [23,26]

$$\begin{aligned}\delta E_n^{(\lambda,L)} &= -\frac{(\alpha k_BT)^{2L+1}}{2J_n+1}\sum_{m\neq n}\left|\langle\Psi_n||Q^{\lambda}_L||\Psi_m\rangle\right|^2\\ &\quad\times F_L\left(\frac{\omega_{mn}}{k_BT}\right), \quad (5)\end{aligned}$$

where J_n is the angular momentum of state $|\Psi_n\rangle$ and

$$\begin{aligned}F_L(y) &= \frac{1}{\pi}\frac{L+1}{L(2L+1)!!(2L-1)!!}\\ &\quad\times\int_0^{\infty}\left(\frac{1}{y+x}+\frac{1}{y-x}\right)\frac{x^{2L+1}}{e^x-1}dx. \quad (6)\end{aligned}$$

Here argument $y = \omega_{mn}/(k_BT) = (\omega_n-\omega_m)/(k_BT)$. The function $F_L(y)$ is a universal function applicable to all the atoms with argument y depending on the range of the atomic parameters. These functions were first introduced by Farley and Wing [23] in the $E1$ case and were extended in a general form by Porsev and Derevianko [26]. In this work, we present simpler forms for the energy-shift expressions. The limit $|y| \gg 1$ which corresponds to the case when the transition energy is much larger than the temperature (k_BT) is of our current interest.

Substituting values from Eq. (A4) (see Appendix A) in Eq. (5), the BBR shift for $L = 1$ can be expressed as

$$\delta E_n^{(\lambda,1)} = -\frac{1}{2}\left[\frac{8\pi^3\alpha^3(k_BT)^4}{45(2J_n+1)}\right]\sum_{m\neq n}\frac{\left|\langle\Psi_n||Q^{\lambda}_1||\Psi_m\rangle\right|^2}{\omega_{mn}}. \quad (7)$$

Using the general definition of the scalar polarizability given by

$$\alpha_n^{Q^{\lambda}_L} = C_n^{Q^{\lambda}_L}\sum_{m\neq n}\frac{\left|\langle\Psi_n||Q^{\lambda}_L||\Psi_m\rangle\right|^2}{E_n-E_m} \quad (8)$$

with $C_n^{Q^{\lambda}_L} = \frac{2}{\alpha^{2(\lambda-1)}(2L+1)(2J_n+1)}$, the BBR shift for the $E1$ channel can be expressed as

$$\begin{aligned}\delta E_n^{E1} &= -\frac{1}{2}\frac{4\pi^3\alpha^3}{15}(k_BT)^4\alpha_n^{E1}\\ &= -\frac{1}{2}\langle E^2_{E1}(\omega)\rangle\alpha_n^{E1}, \quad (9)\end{aligned}$$

whereas for the $M1$ channel it can be reduced to

$$\begin{aligned}\delta E_n^{M1} &= -\frac{1}{2}\frac{4\pi^3\alpha^5}{15}(k_BT)^4\alpha_n^{M1}\\ &= -\frac{1}{2}\alpha^2\langle B^2_{M1}(\omega)\rangle\alpha_n^{M1}, \quad (10)\end{aligned}$$

where α_n^{E1}, α_n^{M1}, $\langle E^2_{E1}(\omega)\rangle$, and $\langle B^2_{M1}(\omega)\rangle$ are the scalar $E1$ polarizability, scalar $M1$ polarizability, the averaged $E1$-induced electric field, and the averaged $M1$-induced magnetic fields, respectively.

Similarly, substituting values from Eq. (A5) (see Appendix A) in Eq. (5), the BBR shift for $L = 2$ comes out as

$$\delta E_n^{(\lambda,2)} = -\frac{1}{2}\left[\frac{16(\alpha\pi)^5(k_BT)^6}{945(2J_n+1)}\right]\sum_{m\neq n}\frac{\left|\langle\Psi_n||Q^{\lambda}_2||\Psi_m\rangle\right|^2}{\omega_{mn}}, \quad (11)$$

which corresponds to the $E2$ and $M2$ channels.

Therefore, the BBR shift for the $E2$ channel is given by

$$\begin{aligned}\delta E_n^{E2} &= -\frac{1}{2}\frac{8(\alpha\pi)^5(k_BT)^6}{189(2J_n+1)}\alpha_n^{E2}\\ &= -\frac{1}{2}\langle E^2_{E2}(\omega)\rangle\alpha_n^{E2}, \quad (12)\end{aligned}$$

where α_n^{E2} is the scalar $E2$ polarizability and $\langle E^2_{E2}(\omega)\rangle$ is the averaged $E2$-induced electric field.

The above energy shifts in the the scale of room temperature $T = 300\ K$ now are given by

$$\delta E_n^{E1}(300\text{K}) = -\frac{1}{2}(831.9\text{V/m})^2\left[\frac{T(\text{K})}{300}\right]^4\alpha_n^{E1}, \quad (13)$$

$$\delta E_n^{M1}(300\text{K}) = -\frac{1}{2}(2.77\times10^{-6}\text{tesla})^2\left[\frac{T(\text{K})}{300}\right]^4\alpha_n^{M1}, \quad (14)$$

and

$$\delta E_n^{E2}(300\text{K}) = -\frac{1}{2}(7.2\times10^{-3}\text{V/m})^2\left[\frac{T(\text{K})}{300}\right]^6\alpha_n^{E2}, \quad (15)$$

due to the $E1$, $M1$, and $E2$ multipoles, respectively, given in Hz where the polarizabilities are taken in a.u..

Accumulating all the above expressions, the BBR shifts in Hz due to both the $M1$ and $E2$ channels for an atomic transition $|\Psi_f\rangle \rightarrow |\Psi_i\rangle$ in the scale of the room temperature turns out to be

$$\delta E^{M1}_{f\rightarrow i} = \delta E^{M1}_f - \delta E^{M1}_i = -\frac{1}{2}(2.77\times 10^{-6}\text{tesla})^2 \times \left[\frac{T(\text{K})}{300}\right]^4 \left(\alpha^{M1}_f - \alpha^{M1}_i\right) \tag{16}$$

and

$$\delta E^{E2}_{f\rightarrow i} = \delta E^{E2}_f - \delta E^{E2}_i = -\frac{1}{2}(7.2\times 10^{-3}\text{V/m})^2 \times \left[\frac{T(\text{K})}{300}\right]^6 \left(\alpha^{E2}_f - \alpha^{E2}_i\right), \tag{17}$$

respectively.

III. METHOD OF CALCULATION

In order to determine $M1$ and $E2$ polarizabilities in the considered systems which have one valence electron each outside closed core, we, first, calculate the Dirac-Fock (DF) wave function ($|\Phi_0\rangle$) for the corresponding closed core and then append the valence orbital (n) to define a new reference state (i.e., $|\Phi_n\rangle = a^\dagger_n|\Phi_0\rangle$) in the spirit of the Fock-space approach. To obtain the exact atomic wave function (ASF) for the closed core with the valence electron n ($|\Psi_n\rangle$), correlation effects through the core-virtual, core-valence, and conjointly the core-virtual and valence-virtual excitations are included in the $|\Phi_n\rangle$ reference state using wave operators Ω_c, Ω_{cn}, and Ω_n, respectively, i.e.,

$$|\Psi_n\rangle = a^\dagger_n\Omega_c|\Phi_0\rangle + \Omega_{cn}|\Phi_n\rangle + \Omega_n|\Phi_n\rangle. \tag{18}$$

We adopt the relativistic coupled-cluster (RCC) method in the Fock-space representation to determine ASFs. With T and S_n representing excitation operators for the electrons in the closed core and for the valence electron n in conjunction with the closed core, respectively, the above ASF in the RCC framework can be encapsulated in a form [12,13,27,28,36–38]

$$|\Psi_n\rangle = e^T\{1+S_n\}|\Phi_n\rangle, \tag{19}$$

where $|\Psi_0\rangle = \Omega_c|\Phi_0\rangle = e^T|\Phi_0\rangle$ can be treated as ASF for the closed core, while other wave operators are given by $\Omega_{cn}|\Phi_n\rangle = e^{T_n}|\Phi_n\rangle$ and $\Omega_n|\Phi_n\rangle = e^T S_n|\Phi_n\rangle$. Subscript n is used for T_n to represent Ω_{cn} which implies that the T operator also involves excitations of the core electrons to the valence orbital n. All these correlation effects are coupled in the course of the $|\Psi_n\rangle$ ASF determination.

The equations determining the coupled-cluster amplitudes and energies are accustomed in compact forms as

$$\left\langle\Phi^K_0\right|\{\widehat{He^T}\}|\Phi_0\rangle = \delta_{0,K}\Delta E_{\text{corr}} \tag{20}$$

and

$$\left\langle\Phi^K_n\right|\{\widehat{He^T}\}\{1+S_n\}|\Phi_n\rangle = \left\langle\Phi^K_n\right|1+S_n|\Phi_n\rangle \times \langle\Phi_n|\{\widehat{He^T}\}\{1+S_n\}|\Phi_n\rangle = \left\langle\Phi^K_n\right|\delta_{n,K}+S_n|\Phi_n\rangle\Delta E_n, \tag{21}$$

where $K = 1,\ 2\ldots$ represent the single, double, and so on, excited configurations, respectively, with respect to their corresponding reference states in both the equations, $\widehat{He^T}$ denotes the connected terms of the Dirac-Coulomb (DC) Hamiltonian (H) with the T operators, and ΔE_{corr} and ΔE_n are the correlation energy for the closed core and the energy required to attach the valence electron n to the closed core [which is negative of the ionization potential (IP) of the valence electron n], respectively. It can be noted that the reference states $|\Phi_0\rangle$ in Eq. (20) and $|\Phi_n\rangle$ in Eq. (21) contain different numbers of particles, hence, the Hamiltonian used in the respective equations describe different numbers of particles in our Fock-space representation. We have considered here contributions only from the singly and doubly excited states by defining T and S_n operators as

$$T = T_1 + T_2 \quad \text{and} \quad S_n = S_{1n} + S_{2n}. \tag{22}$$

To improve the quality of the results, we also construct important valence triple excitations by contracting T_2 and S_{2n} operators with the Coulomb interaction operator (V) in a perturbative procedure in the same spirit as discussed in some of the earlier works (e.g., see Refs. [12,13,27,28,36–39]) and include their contributions to ΔE_n in the above equations self-consistently. This approach is commonly known as the CCSD(T) method.

To calculate the scalar polarizabilities, it is precedence to adopt an approach similar to [27,28] or it would be prudent to follow a procedure given in Ref. [29]. Such approaches may be required to achieve better accuracies. Procuring the derivations in Eq. (B2) (see Appendix B), we can now write

$$\alpha^{Q^\lambda_L}_n = \alpha^{Q^\lambda_L}_n(c) + \alpha^{Q^\lambda_L}_n(nc) + \alpha^{Q^\lambda_L}_n(n), \tag{23}$$

where $\alpha^{Q^\lambda_L}_n(c)$, $\alpha^{Q^\lambda_L}_n(nc)$, and $\alpha^{Q^\lambda_L}_n(n)$ are referred to as core, core-valence, and valence correlation contributions, respectively.

In the sum-over-states approach as given in Eq. (8), it is convenient to determine the low-lying singly excited states $|\Psi_m\rangle$ with respect to the $|\Psi_n\rangle$ states of our interest for both the considered ions using the above RCC method. Contributions from these states correspond to the above-mentioned valence correlation contributions and are the dominant ones compared to the contributions arising from higher-level excited states which can be estimated from a lower-order perturbation theory. In contrast to this contribution, it is not possible to estimate the core and core-valence correlation contributions in the sum-over-states approach. As stated above, the RCC methods described in Refs. [27–29] would be more suitable to account these contributions rigorously. Nevertheless, reasonably accurate core and core-valence contributions are sufficient enough for estimation of the BBR shifts, which is the primary intent of the work. This is for two reasons: First, the core correlation effect may be notable but in the BBR shift estimation this contribution cancels out between two states involved in a transition. Second, it is observed in the earlier works that the core-valence contributions are minuscule in the dipole polarizability calculations [24,25,27,28], which is also the case for the considered multipoles, as has been found below. So it is not necessary to employ a powerful method at the cost

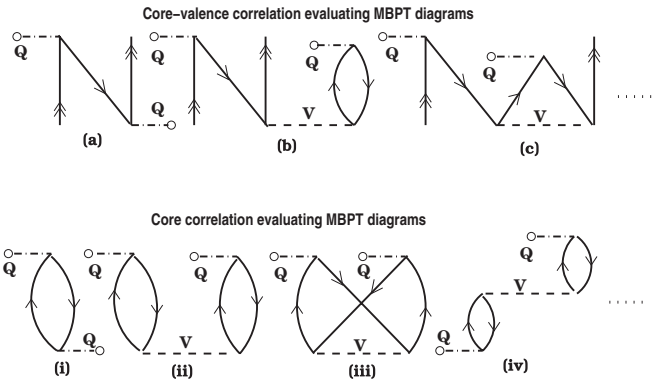

FIG. 1. Few important many-body perturbation theory (MBPT) diagrams used for the core-valence and core correlations estimation.

of heavy computation to determine these small contributions. We determine both the core and core-valence correlation contributions to the $M1$ and $E2$ polarizabilities using the third-order relativistic many-body perturbation theory [MBPT(3)]. In this approach, we rewrite Eq. (8) in a form similar to Refs. [40,41] following the derivation given in Appendix C as

$$\alpha_n^{Q_L^\lambda} = \frac{2}{\alpha^{2(\lambda-1)}} \langle \Psi_n | Q_L^\lambda | \Psi_n^{(1)} \rangle, \tag{24}$$

where $|\Psi_n^{(1)}\rangle$ can be obtained by solving the following inhomogeneous equation:

$$(H - E_n)|\Psi_n^{(1)}\rangle = (E_n^{(1)} - Q_L^\lambda)|\Psi_n\rangle, \tag{25}$$

with $E_n^{(1)} = \langle \Psi_n | Q_L^\lambda | \Psi_n \rangle$, which is similar to the first-order perturbation equation. Some of the important diagrams representing this equation for the core and core-valence correlation effects evaluation are shown in Fig. 1.

The reduced transition matrix element of a physical operator Q_L^λ between $|\Psi_f\rangle$ and $|\Psi_i\rangle$ in our approach is calculated using the expression

$$\frac{\langle \Psi_f || Q_L^\lambda || \Psi_i \rangle}{\sqrt{\langle \Psi_f | \Psi_f \rangle \langle \Psi_i | \Psi_i \rangle}} = \frac{\langle \Phi_f || \{1 + S_f^\dagger\} \overline{Q_L^\lambda} \{1 + S_i\} || \Phi_i \rangle}{\sqrt{\mathcal{N}_f \mathcal{N}_i}}, \tag{26}$$

where $\overline{Q_L^\lambda} = e^{T^\dagger} Q_L^\lambda e^T$ and $\mathcal{N}_n = \langle \Phi_n | e^{T^\dagger} e^T + S_n^\dagger e^{T^\dagger} e^T S_n | \Phi_n \rangle$ involve two nontruncating series in the above expression. We have mentioned concisely the procedure for calculating these expressions in the Appendix of Ref. [36]. We evaluate them keeping terms at least up to fourth order in Coulomb interaction.

The single-particle orbital reduced matrix elements for the corresponding $Q_L^\lambda = \sum q_L^\lambda$ operators are as follows:

$$\langle \kappa_f || q_1^0 || \kappa_i \rangle = (\kappa_f + \kappa_i) \langle -\kappa_f || C^{(1)} || \kappa_i \rangle \times \int_0^\infty dr r [P_f(r) Q_i(r) + Q_f(r) P_i(r)] \tag{27}$$

and

$$\langle \kappa_f || q_2^1 || \kappa_i \rangle = \langle \kappa_f || C^{(2)} || \kappa_i \rangle \times \int_0^\infty dr r^2 [P_f(r) P_i(r) + Q_f(r) Q_i(r)], \tag{28}$$

where $P(r)$ and $Q(r)$ represent the radial parts of the large and small components of the single-particle Dirac orbitals, respectively. The reduced Racah coefficients are given by

$$\langle \kappa_f || C^{(k)} || \kappa_i \rangle = (-1)^{j_f + 1/2} \sqrt{(2j_f + 1)(2j_i + 1)} \times \begin{pmatrix} j_f & k & j_i \\ 1/2 & 0 & -1/2 \end{pmatrix} \pi(l_{\kappa_f}, k, l_{\kappa_i}), \tag{29}$$

with

$$\pi(l,m,l') = \begin{cases} 1 & \text{for } l + m + l' = \text{even} \\ 0 & \text{otherwise.} \end{cases} \tag{30}$$

We have used Gaussian-type orbitals (GTOs) to construct the single-particle orbitals for the Dirac-Fock ($|\Phi_0\rangle$) wave-function calculation. The large and small components of the Dirac orbitals in this case are expressed as

$$P_\kappa(r) = \sum_k c_k^P r^{l_\kappa} e^{-\alpha_k r^2} \tag{31}$$

and

$$Q_\kappa(r) = \sum_k c_k^Q r^{l_\kappa} \left(\frac{d}{dr} + \frac{\kappa}{r} \right) e^{-\alpha_k r^2}, \tag{32}$$

where the summation over k is for the total number of GTOs used in each symmetry and c_k^P and c_k^Q are the normalization constants for the large and small components, respectively, and we use the $(\frac{d}{dr} + \frac{\kappa}{r})$ operator to expand the small component Dirac orbitals to maintain the kinetic balance condition with its large component. In the present calculations, we have considered nine relativistic symmetries (up to g symmetry) and 28 GTOs for each symmetry to generate the orbitals. In order to optimize the exponents to describe orbitals from various symmetries in a smooth manner, we use the even tempering condition

$$\alpha_k = \alpha_0 \beta^{k-1}, \tag{33}$$

where α_0 and β are two arbitrary parameters that are chosen suitably for different symmetries.

We have considered $\alpha_0 = 7.5 \times 10^{-4}$ for all the symmetries and βs are optimized to be 2.56, 2.58, 2.61, 2.75, and 2.83 for the s, p, d, f, and g orbitals, respectively. For the RCC calculations, we have considered excitations up to first $16s$, $16p$, $16d$, $14f$, and $13g$ orbitals while contributions from other virtual orbitals having large energies are neglected.

IV. RESULTS AND DISCUSSIONS

To verify how accurately the present method can reproduce energies and $E_n^{(1),\lambda}$s, we have given these results in Table I for the considered states in both Ca^+ and Sr^+ and compared them with the corresponding available experimental values. As seen in this table, our results are in sufficient agreement with the measured values. Therefore, we can expect the other quantities estimated using our method to be of similar accuracy. As has been emphasized before, precise estimation of the BBR shifts due to $M1$ and $E2$ transitions in Ca^+ and Sr^+ are the focus of this work. There are two uncertainties in these estimations: (i) the errors associated with the considered excitation energies (EEs) and (ii) the inaccuracies from the estimated transition matrix elements. As can be noted from Table I, our calculated

TABLE I. Experimental and calculated ionization potentials (E_n) in cm^{-1} and $E_n^{(1),\lambda}$ in a.u. for different states in Ca^+ and Sr^+.

	State	Experiment		This work		
	$\|\Psi_n\rangle$	E_n [42]	$E_n^{(1),1}$	E_n	$E_n^{(1),0}$	$E_n^{(1),1}$
Ca^+	$4s_{1/2}$	95751.87		95758.57	0.0073	0.0
	$3d_{5/2}$	82040.99	1.83(1)[a]	80983.28	0.0219	1.894
Sr^+	$5s_{1/2}$	88965.18		88982.51	0.0073	0.0
	$4d_{5/2}$	74128.94	2.6(3)[b]	73554.86	0.0219	2.945

[a]Reference [43].
[b]Reference [44].

energies are in reasonable agreement with the experimental values. However, the associated uncertainties are a little large for the $d_{5/2}$ states. For this reason and to abate the uncertainties in the evaluation of the BBR shift for the atomic clock application, we use the experimental EEs from the NIST database [42] for the important singly excited states in the valence contribution. In Tables II and III, contributions to the $M1$ and $E2$ matrix element calculations are given in terms of important RCC terms for various transitions in Ca^+ and Sr^+, respectively. We also estimate uncertainties from the neglected contributions as (i) the Breit interaction, (ii) the neglected triple excitations, and (iii) the inactive orbitals that are not accounted for in the RCC method (given as contributions from basis).

TABLE II. Contributions to the $M1$ and $E2$ matrix elements from the important RCC terms containing the lowest-order contributions (in a.u.) in Ca^+. Estimated uncertainties from various neglected contributions (absolute values) are also given. Numbers after four decimal places are neglected.

								Uncertainty (absolute values)		
Transition	DF	$\overline{Q_L^\lambda}$-DF	$\overline{Q_L^\lambda} S_{1i}$	$S_{1f}^\dagger \overline{Q_L^\lambda}$	$\overline{Q_L^\lambda} S_{2i}$	$S_{2f}^\dagger \overline{Q_L^\lambda}$	Others	Breit	Triples	Basis
					$M1$ channels					
$4s_{1/2} \rightarrow 5s_{1/2}$	∼0.0	0.0012	0.1044	−0.0898	∼0.0	∼0.0	−.0140	∼0.0	∼0.0	0.0003
$4s_{1/2} \rightarrow 6s_{1/2}$	∼0.0	0.0008	0.0482	−0.0419	∼0.0	∼0.0	0.0058	∼0.0	∼0.0	0.0002
$4s_{1/2} \rightarrow 3d_{3/2}$	∼0.0	0.0006	0.0001	∼0.0	∼0.0	∼0.0	0.0001	∼0.0	∼0.0	0.0001
$4s_{1/2} \rightarrow 4d_{3/2}$	∼0.0	0.0003	∼0.0	∼0.0	∼0.0	∼0.0	∼0.0	∼0.0	∼0.0	0.0001
$4s_{1/2} \rightarrow 5d_{3/2}$	∼0.0	0.0001	∼0.0	∼0.0	∼0.0	∼0.0	∼0.0	∼0.0	∼0.0	0.0001
$4s_{1/2} \rightarrow 6d_{3/2}$	∼0.0	0.0001	∼0.0	∼0.0	∼0.0	∼0.0	∼0.0	∼0.0	∼0.0	0.0001
$3d_{5/2} \rightarrow 3d_{3/2}$	1.5491	−0.0129	−0.0014	−0.0010	0.0001	−0.0001	0.0095	0.0001	0.0017	0.0065
$3d_{5/2} \rightarrow 4d_{3/2}$	0.0011	0.0025	0.1466	−0.1261	∼0.0	∼0.0	−0.0201	0.0002	∼0.0	0.0008
$3d_{5/2} \rightarrow 5d_{3/2}$	0.0001	0.0040	0.0611	−0.0583	∼0.0	∼0.0	−0.0039	0.0001	∼0.0	0.0009
$3d_{5/2} \rightarrow 6d_{3/2}$	∼0.0	0.0030	0.0374	−0.0381	∼0.0	∼0.0	0.0007	0.0001	∼0.0	0.0009
$3d_{5/2} \rightarrow 4d_{5/2}$	∼0.0	0.0014	0.8215	−0.7085	∼0.0	∼0.0	−0.1104	∼0.0	∼0.0	0.0014
$3d_{5/2} \rightarrow 5d_{5/2}$	∼0.0	0.0098	−0.3426	0.3284	∼0.0	∼0.0	0.0232	∼0.0	0.0001	0.0017
$3d_{5/2} \rightarrow 6d_{5/2}$	∼0.0	0.0035	0.2101	−0.2148	∼0.0	∼0.0	0.0032	∼0.0	∼0.0	0.0012
$3d_{5/2} \rightarrow 5g_{7/2}$	∼0.0	∼0.0	∼0.0	∼0.0	∼0.0	∼0.0	∼0.0	∼0.0	∼0.0	∼0.0
$3d_{5/2} \rightarrow 6g_{7/2}$	∼0.0	∼0.0	∼0.0	∼0.0	∼0.0	∼0.0	∼0.0	∼0.0	∼0.0	∼0.0
					$E2$ channels					
$4s_{1/2} \rightarrow 3d_{3/2}$	9.7672	−0.0075	−1.4539	−0.2751	−0.0431	−0.0072	0.1396	0.0071	0.0153	0.0276
$4s_{1/2} \rightarrow 4d_{3/2}$	12.7033	−0.0026	1.5117	−1.3596	0.0015	−0.0131	0.3312	0.0092	0.0071	0.0637
$4s_{1/2} \rightarrow 5d_{3/2}$	4.2184	−0.0016	−0.2634	−0.1176	−0.0106	−0.0007	−0.0654	0.0001	0.0045	0.0354
$4s_{1/2} \rightarrow 6d_{3/2}$	2.6120	0.0010	−0.3452	−0.0037	−0.0010	−0.0085	0.0324	0.0008	0.0053	0.0539
$4s_{1/2} \rightarrow 4d_{5/2}$	15.3802	0.0035	1.8448	−1.6652	0.0020	−0.0163	−0.2490	0.0144	0.0301	0.0155
$4s_{1/2} \rightarrow 5d_{5/2}$	5.1556	0.0021	−0.3249	−0.1454	−0.0008	0.0131	0.0503	0.0004	0.0036	0.0460
$4s_{1/2} \rightarrow 6d_{5/2}$	3.3798	0.0014	−0.4239	−0.0052	−0.0012	−0.0106	0.0397	0.0016	0.0031	0.0553
$3d_{5/2} \rightarrow 4s_{1/2}$	12.1082	−0.0099	−0.3377	−1.7472	−0.0076	−0.0530	0.1723	0.0121	0.0152	0.0327
$3d_{5/2} \rightarrow 5s_{1/2}$	7.4423	0.0045	0.6277	−2.9089	0.0003	0.0191	−0.1950	0.0228	0.0011	0.0261
$3d_{5/2} \rightarrow 6s_{1/2}$	1.5126	0.0028	0.0014	−0.3526	0.0002	0.0113	0.0443	0.0020	0.0001	0.0179
$3d_{5/2} \rightarrow 3d_{3/2}$	5.0892	−0.0140	−0.5895	−0.5772	−0.0425	−0.0428	0.0768	0.0073	0.0089	0.0238
$3d_{5/2} \rightarrow 4d_{3/2}$	5.4910	0.0052	0.6682	−1.7138	0.0144	0.0112	−0.1562	0.0098	0.0091	0.0311
$3d_{5/2} \rightarrow 5d_{3/2}$	1.5620	0.0030	−0.1241	−0.1683	0.0092	0.0058	0.0924	0.0011	0.0007	0.0182
$3d_{5/2} \rightarrow 6d_{3/2}$	1.2119	0.0025	−0.1270	−0.0689	0.0067	0.0039	0.0509	0.0006	0.0006	0.0088
$3d_{5/2} \rightarrow 4d_{5/2}$	10.9736	0.0108	1.3324	−3.4267	0.0289	0.0225	−0.3115	0.0172	0.0243	0.0085
$3d_{5/2} \rightarrow 5d_{5/2}$	3.1174	0.0064	−0.2496	−0.3390	0.0184	0.0116	0.1848	0.0023	0.0134	0.0143
$3d_{5/2} \rightarrow 6d_{5/2}$	2.4256	0.0052	−0.2547	−0.1393	0.0134	0.0078	0.1020	0.0015	0.0026	0.0159
$3d_{5/2} \rightarrow 5g_{7/2}$	2.4225	−0.0001	0.0105	−0.8315	−0.0005	−0.0007	−0.0202	0.0221	∼0.0	0.0021
$3d_{5/2} \rightarrow 6g_{7/2}$	1.6175	−0.0006	0.0042	−0.5644	−0.0005	−0.0008	−0.0154	0.0043	∼0.0	0.0057
$3d_{5/2} \rightarrow 5g_{9/2}$	8.5489	−0.0003	0.0372	−2.9400	−0.0018	−0.0026	−0.0714	0.0225	∼0.0	0.0275
$3d_{5/2} \rightarrow 6g_{9/2}$	5.7122	−0.0020	0.0149	−1.9955	−0.0020	−0.0029	−0.0547	0.0151	∼0.0	0.0249

TABLE III. Contributions to the $M1$ and $E2$ matrix elements from the important RCC terms containing the lowest-order contributions (in a.u.) in Sr^+. Estimated uncertainties from various neglected contributions (absolute values) are also given. Numbers after four decimal places are neglected.

Transition	DF	$\overline{Q_L^\lambda}$-DF	$\overline{Q_L^\lambda} S_{1i}$	$S_{1f}^\dagger \overline{Q_L^\lambda}$	$\overline{Q_L^\lambda} S_{2i}$	$S_{2f}^\dagger \overline{Q_L^\lambda}$	Others	Uncertainty (absolute values) Breit	Triples	Basis
					$M1$ channels					
$5s_{1/2} \rightarrow 6s_{1/2}$	∼0.0	0.0011	0.1255	−0.1086	∼0.0	∼0.0	−0.0166	∼0.0	∼0.0	0.0021
$5s_{1/2} \rightarrow 7s_{1/2}$	∼0.0	0.0007	0.0559	−0.0494	∼0.0	∼0.0	−0.0059	∼0.0	∼0.0	0.0013
$5s_{1/2} \rightarrow 8s_{1/2}$	∼0.0	0.0005	0.0345	−0.0294	∼0.0	∼0.0	−0.0046	∼0.0	∼0.0	0.0011
$5s_{1/2} \rightarrow 9s_{1/2}$	∼0.0	0.0004	0.0283	−0.0207	∼0.0	∼0.0	−0.0070	∼0.0	∼0.0	0.0010
$5s_{1/2} \rightarrow 4d_{3/2}$	∼0.0	∼0.0	∼0.0	∼0.0	∼0.0	∼0.0	∼0.0	∼0.0	∼0.0	∼0.0
$5s_{1/2} \rightarrow 5d_{3/2}$	∼0.0	∼0.0	∼0.0	∼0.0	∼0.0	∼0.0	∼0.0	∼0.0	∼0.0	∼0.0
$5s_{1/2} \rightarrow 6d_{3/2}$	∼0.0	∼0.0	∼0.0	∼0.0	∼0.0	∼0.0	∼0.0	∼0.0	∼0.0	∼0.0
$5s_{1/2} \rightarrow 7d_{3/2}$	∼0.0	∼0.0	∼0.0	∼0.0	∼0.0	∼0.0	∼0.0	∼0.0	∼0.0	∼0.0
$4d_{5/2} \rightarrow 4d_{3/2}$	1.5491	−0.0096	−0.0013	∼0.0	0.0004	−0.0003	0.0067	0.0001	0.0007	0.0058
$4d_{5/2} \rightarrow 5d_{3/2}$	0.0052	0.0042	0.1081	−0.0944	∼0.0	0.0001	−0.0142	0.0003	0.0001	0.0023
$4d_{5/2} \rightarrow 6d_{3/2}$	0.0028	0.0028	0.0458	−0.0429	∼0.0	0.0001	−0.0025	0.0002	0.0001	0.0012
$4d_{5/2} \rightarrow 7d_{3/2}$	0.0022	0.0022	0.0306	−0.0301	∼0.0	∼0.0	−0.0009	0.0001	∼0.0	0.0010
$4d_{5/2} \rightarrow 5d_{5/2}$	∼0.0	0.0112	0.5953	−0.5282	∼0.0	∼0.0	−0.0752	∼0.0	∼0.0	0.0013
$4d_{5/2} \rightarrow 6d_{5/2}$	∼0.0	0.0073	0.2535	−0.2416	∼0.0	∼0.0	−0.0162	∼0.0	∼0.0	0.0012
$4d_{5/2} \rightarrow 7d_{5/2}$	∼0.0	0.0059	0.1708	−0.1701	∼0.0	∼0.0	−0.0046	∼0.0	0.0001	0.0010
$4d_{5/2} \rightarrow 5g_{7/2}$	∼0.0	∼0.0	∼0.0	∼0.0	∼0.0	∼0.0	∼0.0	∼0.0	∼0.0	∼0.0
$4d_{5/2} \rightarrow 6g_{7/2}$	∼0.0	∼0.0	∼0.0	∼0.0	∼0.0	∼0.0	∼0.0	∼0.0	∼0.0	∼0.0
					$E2$ channels					
$5s_{1/2} \rightarrow 4d_{3/2}$	12.9754	0.0052	−1.2114	−0.4403	−0.0685	−0.0343	0.0258	0.0093	0.0057	0.0551
$5s_{1/2} \rightarrow 5d_{3/2}$	13.4672	0.0022	1.4970	−1.8951	0.0080	−0.0100	−0.2047	0.0138	0.0061	0.0601
$5s_{1/2} \rightarrow 6d_{3/2}$	5.0007	0.0017	−0.03153	−0.2551	0.0103	−0.0030	0.0407	0.0013	0.0007	0.0482
$5s_{1/2} \rightarrow 7d_{3/2}$	3.1389	0.0015	−0.1127	−0.0122	0.0018	−0.0097	−0.2007	0.0002	0.0002	0.0421
$5s_{1/2} \rightarrow 4d_{5/2}$	15.9812	−0.0074	−1.4408	−0.5456	−0.0849	−0.0360	0.0435	0.0169	0.0086	0.0545
$5s_{1/2} \rightarrow 5d_{5/2}$	16.3892	0.0032	1.8133	−2.3191	0.0103	−0.0139	0.7570	0.0231	0.0067	0.0602
$5s_{1/2} \rightarrow 6d_{5/2}$	6.2615	0.0024	−0.0294	−0.3205	0.0039	−0.0136	0.0657	0.0022	0.0008	0.0570
$5s_{1/2} \rightarrow 7d_{5/2}$	3.8933	0.0022	−0.1278	−0.0193	0.0023	−0.0127	0.0260	0.0005	0.0002	0.0393
$4d_{5/2} \rightarrow 6s_{1/2}$	9.8215	0.0032	1.0103	−2.9297	0.0111	0.0275	−0.2295	0.0357	0.0007	0.0136
$4d_{5/2} \rightarrow 7s_{1/2}$	2.0783	0.0019	0.0015	−0.2697	0.0073	0.0154	0.0625	0.0028	0.0003	0.0169
$4d_{5/2} \rightarrow 8s_{1/2}$	0.9773	0.0013	0.0328	−0.0913	0.0054	0.0099	0.0268	0.0010	0.0001	0.0089
$4d_{5/2} \rightarrow 9s_{1/2}$	0.6311	0.0010	0.1267	−0.0603	0.0050	0.0074	0.0058	0.0009	∼0.0	0.0091
$4d_{5/2} \rightarrow 4d_{3/2}$	7.2609	−0.0188	−0.5495	−0.5281	−0.0656	−0.0678	0.0510	0.0111	0.0005	0.0484
$4d_{5/2} \rightarrow 5d_{3/2}$	6.6393	0.0074	0.7200	−1.6470	0.0232	0.0174	−0.1326	0.0142	0.0002	0.0456
$4d_{5/2} \rightarrow 6d_{3/2}$	1.9530	0.0046	−0.0594	−0.1594	0.0154	0.0092	0.0616	0.0016	0.0001	0.0183
$4d_{5/2} \rightarrow 7d_{3/2}$	1.2132	0.0037	−0.0812	−0.0485	0.0126	0.0068	0.0284	0.0006	∼0.0	0.0094
$4d_{5/2} \rightarrow 5d_{5/2}$	13.1991	0.0150	1.4235	−3.2899	0.0471	0.0345	−0.2622	0.0237	0.0065	0.0398
$4d_{5/2} \rightarrow 6d_{5/2}$	3.9065	0.0093	−0.1118	−0.3292	0.0312	−0.0184	0.1574	0.0032	0.0008	0.0460
$4d_{5/2} \rightarrow 7d_{5/2}$	2.4310	0.0075	−0.1561	−0.1027	0.0254	0.0136	0.0561	0.0055	0.0003	0.0242
$4d_{5/2} \rightarrow 5g_{7/2}$	3.6591	−0.0002	0.0264	−0.9298	−0.0016	−0.0022	−0.0252	0.0109	0.0001	0.0190
$4d_{5/2} \rightarrow 6g_{7/2}$	2.7932	0.0003	0.0086	−0.5747	−0.0016	−0.0023	−0.0166	0.0068	∼0.0	0.0132
$4d_{5/2} \rightarrow 5g_{9/2}$	12.9370	−0.0006	0.0932	−3.2873	−0.0056	−0.0078	−0.0893	0.0385	∼0.0	0.0315
$4d_{5/2} \rightarrow 6g_{9/2}$	9.8755	−0.0009	0.0305	−2.0320	−0.0059	−0.0083	−0.0560	0.0241	∼0.0	0.0359

Contributions from the first and third sources are estimated using the MBPT(2) method and the second contributions are estimated contracting the perturbatively constructed triple excitation operators with the conjugate of the T_2 operators, which are used to improve the calculations of the energies but are not available explicitly for the property evaluation, as shown in Fig. 2. Contributions in estimating the scalar $M1$ and $E2$ polarizabilities from the above matrix elements with their uncertainties are given in Tables IV, V, VI, and VII. Also, the contributions from the higher singly and doubly excited states whose matrix elements are not given in the above table are reported as α_{tail}. These contributions and the contributions from core and core-valence states are estimated using MBPT(3) method. It can be noted from Tables IV, V, VI, and VII that α_{tail} contributions are diminutive and these results can be calculated with reasonable accuracy using the

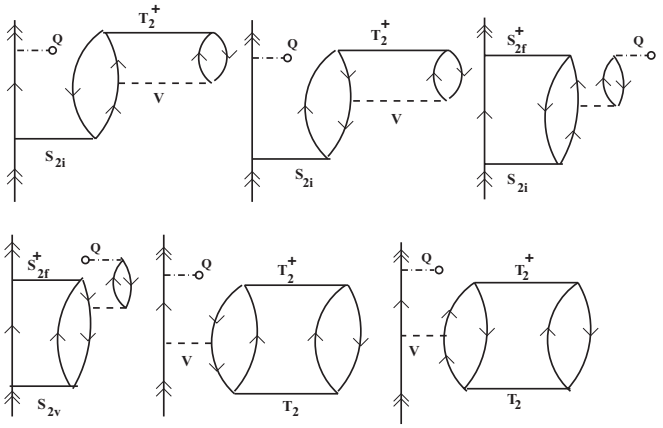

FIG. 2. Some of the important diagrams which along with their conjugates are used to estimate the contributions from the neglected triple excitations.

MBPT(3) method. The large uncertainties in the determination of the polarizabilities for a given state $|\Psi_n\rangle$ are from the lower valence states and the uncertainties are evaluated for each of these intermediate state $|\Psi_m\rangle$ using the relation

$$\delta\alpha_n^{Q_L^\lambda}(m) = \frac{1}{\alpha^{2(\lambda-1)}}\sum_{m\neq n}\langle\Psi_n||Q_L^\lambda||\Psi_m\rangle\frac{1}{2L+1}\frac{1}{2J_n+1} \times\frac{\langle\Psi_n||Q_L^\lambda||\Psi_m\rangle}{E_n-E_m}\delta\left(\langle\Psi_n||Q_L^\lambda||\Psi_k\rangle\right) = 2\times\alpha_n^{Q_L^\lambda}(m)\frac{\delta\left(\langle\Psi_n||Q_L^\lambda||\Psi_m\rangle\right)}{\langle\Psi_n||Q_L^\lambda||\Psi_m\rangle}, \quad (34)$$

where $\langle\Psi_n||Q_L^\lambda||\Psi_m\rangle$ and $\delta\langle\Psi_n||Q_L^\lambda||\Psi_m\rangle$ are the absolute value and uncertainties of the matrix elements, respectively. Finally, uncertainties to the polarizability $\delta\alpha_n^{Q_L^\lambda}(m)$ from each intermediate state are added using the quadrature formula to estimate the net uncertainty in $\alpha_n^{Q_L^\lambda}$.

We, first, present the static scalar α^{M1} polarizabilities in the Ca^+ and Sr^+ ions in Tables IV and V, respectively, for both the ground and $d_{5/2}$ states. As seen in these tables, α^{M1}s are very small for the corresponding ground states in both the ions; however, they are reported in this paper for completeness of the results. Contributions from the core correlations are the largest in determining these results and they will be canceled while estimating the BBR shifts due to the $M1$ multipole. Therefore, the ground-state $M1$ polarizability contributions in the considered ions can be neglected. Essentially, the contributions to the α^{M1} polarizabilities in the $d_{5/2}$ states are overwhelmingly dominant due to the very small energy gap of their fine-structure partner states and the contributions from all other states are small. The $M1$ matrix elements between the $d_{3/2}$-$d_{5/2}$ transitions in the considered ions were also reported earlier by us [45] and they seem to be very consistent. From our calculations, we obtain α^{M1} for the $3d_{5/2}$ and $4d_{5/2}$ states as $-957(6)$ a.u. and $-208(2)$ a.u. in the Ca^+ and Sr^+ ions, respectively.

We now turn to the α^{E2} results. Our calculated results for the ground and $3d_{5/2}$ states in Ca^+ are given in Table VI. Both results are comparatively large with opposite signs. The

TABLE IV. Contributions to the $4s_{1/2}$ and $3d_{5/2}$ scalar (α^{M1}) static polarizabilities in Ca^+ and their uncertainties in a_0^3 (a.u.). The values of the corresponding $|\langle\psi_n||Q_0^1||\psi_m\rangle|/\alpha$ matrix elements are given in ea_0 (a.u.).

Transition		Amplitude	α^{M1}
	α_n		
$4s_{1/2}\rightarrow$	$5s_{1/2}$	0.0018(3)	$0.4(1)\times10^{-5}$
	$6s_{1/2}$	0.0013(2)	$1.7(5)\times10^{-6}$
	$3d_{3/2}$	0.0008(1)	$3.1(8)\times10^{-6}$
	$4d_{3/2}$	0.0003(1)	$0.9(7)\times10^{-7}$
	$5d_{3/2}$	0.0001(1)	$0.8(20)\times10^{-8}$
	$6d_{3/2}$	0.0003(1)	$0.6(5)\times10^{-7}$
	α_c		$5.0(2)\times10^{-5}$
	α_{cn}		$-1.4(3)\times10^{-8}$
	$\alpha_{\rm tail}$		$1.0(2)\times10^{-8}$
	$\alpha_{\rm total}$		$5.9(3)\times10^{-5}$
	α_n		
$3d_{5/2}\rightarrow$	$3d_{3/2}$	1.543(5)	$-957(6)$
	$4d_{3/2}$	0.004(1)	$8(4)\times10^{-6}$
	$5d_{3/2}$	0.004(1)	$8(4)\times10^{-6}$
	$6d_{3/2}$	0.003(1)	$2(2)\times10^{-6}$
	$4d_{5/2}$	0.004(1)	$8(4)\times10^{-6}$
	$5d_{5/2}$	0.009(2)	$3(1)\times10^{-5}$
	$6d_{5/2}$	0.002(1)	$1(1)\times10^{-6}$
	$5g_{7/2}$	3.2×10^{-7}	~0
	$6g_{7/2}$	4.6×10^{-7}	~0
	α_c		$5.0(2)\times10^{-5}$
	α_{cn}		0.0
	$\alpha_{\rm tail}$		$-5.0(6)\times10^{-6}$
	$\alpha_{\rm total}$		$-957(6)$

largest contribution to the ground-state polarizability comes from the $3d$ states followed by the $4d$ states. The core contribution is comparatively small and the α_{cn} contribution to the ground-state polarizability is zero due to the absence of occupied d states in Ca^+. There are two more calculations available in the literature on the same using the RCC methods with different levels of approximations [46,47]. The results reported in Ref. [46] are *ab initio* and are obtained from a linear response theory–based calculation. A linear approximation in the RCC method is being considered to evaluate the corresponding transition matrix elements for the estimation of the ground-state polarizability in Ref. [47] using a sum-over-states approach as in the present work. All the results are of the same order in magnitude. The *ab initio* result seems to be a little lower than the results obtained from the sum-over-states approach due to the additional uncertainties from the calculated energies which justifies the use of the experimental energies in these calculations. However, it should be noted that the differences in these results will not alter the BBR shift results which is apparent from the following finding on the $E2$ polarizability contributions. To our knowledge, no other quadrupole polarizability result is available for the $3d_{5/2}$ state in Ca^+ to compare with ours. Again, the contribution from its fine-structure partner is the decisive factor for the final result followed by a significant contribution from the ground state.

In Table VII, we present the α^{E2} results for the ground and $4d_{5/2}$ states in Sr^+. The magnitudes of the ground-state result

TABLE V. Contributions to the $5s_{1/2}$ and $4d_{5/2}$ scalar (α^{M1}) static polarizabilities in Sr^+ and their uncertainties in a_0^3 (a.u.). The values of the corresponding $|\langle\psi_n||Q_0^1||\psi_m\rangle|/\alpha$ matrix elements are given in ea_0 (a.u.).

Transition		Amplitude	α^{M1}
α_n			
$5s_{1/2} \rightarrow$	$6s_{1/2}$	$1.35(2) \times 10^{-3}$	$2.79(8) \times 10^{-6}$
	$7s_{1/2}$	$1.24(1) \times 10^{-3}$	$1.73(3) \times 10^{-6}$
	$8s_{1/2}$	$1.00(1) \times 10^{-3}$	$1.0(2) \times 10^{-6}$
	$9s_{1/2}$	$1.00(1) \times 10^{-3}$	$9.4(2) \times 10^{-7}$
	$4d_{3/2}$	$5.0(3) \times 10^{-5}$	$1.3(2) \times 10^{-8}$
	$5d_{3/2}$	$1.0(1) \times 10^{-5}$	$1.4(3) \times 10^{-10}$
	$6d_{3/2}$	$1.0(1) \times 10^{-6}$	$1.1(2) \times 10^{-12}$
	$7d_{3/2}$	$3.0(2) \times 10^{-6}$	$8.8(6) \times 10^{-12}$
α_c			$1.0(1) \times 10^{-3}$
α_{cn}			$-2(1) \times 10^{-8}$
α_{tail}			$1.0(1) \times 10^{-8}$
α_{total}			$1.0(1) \times 10^{-3}$
α_n			
$4d_{5/2} \rightarrow$	$4d_{3/2}$	1.545(6)	$-208(2)$
	$5d_{3/2}$	0.009(2)	$5(2) \times 10^{-5}$
	$6d_{3/2}$	0.006(1)	$1.5(5) \times 10^{-5}$
	$7d_{3/2}$	0.004(1)	$7(3) \times 10^{-6}$
	$5d_{5/2}$	0.003(1)	$6(4) \times 10^{-6}$
	$6d_{5/2}$	0.003(1)	$4(3) \times 10^{-6}$
	$7d_{5/2}$	0.002(1)	$2(2) \times 10^{-6}$
	$5g_{7/2}$	$3.2(5) \times 10^{-7}$	~ 0
	$6g_{7/2}$	$3.0(4) \times 10^{-7}$	~ 0
α_c			$1.0(1) \times 10^{-3}$
α_{cn}			$-2.5(2) \times 10^{-7}$
α_{tail}			$-1.5(1) \times 10^{-7}$
α_{total}			$-208(2)$

TABLE VI. Contributions to the $4s_{1/2}$ and $3d_{5/2}$ scalar (α^{E2}) static polarizabilities in Ca^+ and their uncertainties in a_0^5 (a.u.). The values of the corresponding $|\langle\psi_n||Q_1^2||\psi_m\rangle|$ matrix elements are given in ea_0^2 (a.u.).

Transition		Amplitude	α^{E2}
α_n			
$4s_{1/2} \rightarrow$	$3d_{3/2}$	8.12(5)	212(3)
	$4d_{3/2}$	12.51(8)	121(2)
	$5d_{3/2}$	3.89(4)	9.1(2)
	$6d_{3/2}$	2.44(6)	16.2(4)
	$3d_{5/2}$	9.97(6)	318(3)
	$4d_{5/2}$	15.30(9)	181(2)
	$5d_{5/2}$	4.75(5)	13.6(3)
	$6d_{5/2}$	2.98(6)	24.2(4)
α_c			6.15(8)
α_{cn}			0.0
α_{tail}			5.36(5)
α_{total}			906(5)
Other works			712.91,[a] 871[b]
α_n			
$3d_{5/2} \rightarrow$	$4s_{1/2}$	9.97(6)	$-106(1)$
	$5s_{1/2}$	4.99(5)	9.4(2)
	$6s_{1/2}$	1.22(2)	0.38(1)
	$3d_{3/2}$	3.90(4)	$-3657(75)$
	$4d_{3/2}$	4.32(5)	6.3(1)
	$5d_{3/2}$	1.38(2)	0.47(1)
	$6d_{3/2}$	1.08(1)	0.25(5)
	$4d_{5/2}$	8.63(5)	25.2(3)
	$5d_{5/2}$	2.75(3)	1.87(4)
	$6d_{5/2}$	2.16(2)	1.02(2)
	$5g_{7/2}$	1.58(2)	0.56(1)
	$6g_{7/2}$	1.04(1)	0.210(4)
	$5g_{9/2}$	5.57(5)	7.0(1)
	$6g_{9/2}$	3.67(4)	2.62(6)
α_c			6.15(8)
α_{cn}			0.18(2)
α_{tail}			$-4.29(7)$
α_{total}			$-3706(75)$

[a]Reference [46].
[b]Reference [47].

in this ion is larger than Ca^+, while for the corresponding $d_{5/2}$ state it is the other way around. There are no results available, to the best of our knowledge, with which to compare our results. The trend of the contributions from different transitions is almost similar for corresponding states in both ions.

Using the above values of the polarizabilities, we obtain the BBR shift due to the $M1$ multipole for the $4s\ ^2S_{1/2} \rightarrow 3d\ ^2D_{5/2}$ transition in Ca^+ at the room temperature (300 K) to be $4.38(3) \times 10^{-4}$ Hz. Similarly, this result comes out to be $9.50(7) \times 10^{-5}$ Hz for the $5s\ ^2S_{1/2} \rightarrow 4d\ ^2D_{5/2}$ transition in Sr^+. Contributions from the $E2$ multipole are very small and below the uncertainties of the above results and, hence, can be neglected for the present purposes of this work. However, the reported quadrupole polarizabilities for all the considered states may be useful elsewhere. For comparison, it should be noted that the BBR shifts due to the $E1$ multipole are 0.38(1) Hz [28,47] and 0.22(1) Hz [27] in the corresponding transitions in Ca^+ and Sr^+, respectively.

V. CONCLUSION

In summary, we have estimated the blackbody radiation shifts due to the magnetic dipole and electric quadrupole multipoles for the $4s\ ^2S_{1/2} \rightarrow 3d\ ^2D_{5/2}$ and $5s\ ^2S_{1/2} \rightarrow 4d\ ^2D_{5/2}$ transitions in the singly ionized calcium and strontium, respectively. The contribution due to the former is the decisive in this case. Nevertheless, the reported polarizabilities for the considered states which are rarely studied in the above ions may also be useful for other purposes. It may be imperative to contemplate the reported shifts which are given as $4.38(3) \times 10^{-4}$ Hz and $9.50(7) \times 10^{-5}$ Hz in the considered ions to achieve the 10^{-18} precision uncertainty in the proposed clock experiments.

ACKNOWLEDGMENTS

The work of B.A. was supported by the Department of Science and Technology, India. Computations were carried out using the 3TFLOP HPC Cluster at Physical Research Laboratory, Ahmedabad.

TABLE VII. Contributions to the $5s_{1/2}$ and $4d_{5/2}$ scalar (α_0^{E2}) static polarizabilities in Sr^+ and their uncertainties in a_0^5 (a.u.). The values of the corresponding $|\langle\psi_n||Q_1^2||\psi_m\rangle|$ matrix elements are given in ea_0^2 (a.u.).

Transition		Amplitude	α^{E2}
	α_n		
$5s_{1/2} \rightarrow$	$4d_{3/2}$	11.25(7)	382(5)
	$5d_{3/2}$	12.87(8)	136(2)
	$6d_{3/2}$	5.00(5)	16.2(3)
	$7d_{3/2}$	3.11(4)	5.7(1)
	$4d_{5/2}$	13.91(8)	572(6)
	$5d_{5/2}$	15.64(9)	201(2)
	$6d_{5/2}$	5.97(6)	23.3(4)
	$7d_{5/2}$	3.76(4)	8.3(1)
	α_c		14.50(9)
	α_{cn}		$-1.7(2) \times 10^{-8}$
	α_{tail}		6.35(8)
	α_{total}		1366(9)
	α_n		
$4d_{5/2} \rightarrow$	$5s_{1/2}$	13.91(8)	−191(2)
	$6s_{1/2}$	7.71(5)	274(3)
	$7s_{1/2}$	1.90(2)	1.05(2)
	$8s_{1/2}$	0.96(1)	0.231(5)
	$9s_{1/2}$	0.72(1)	0.119(4)
	$4d_{3/2}$	6.08(6)	−1930(38)
	$5d_{3/2}$	5.63(6)	12.1(3)
	$6d_{3/2}$	1.83(2)	0.92(2)
	$7d_{3/2}$	1.14(1)	0.315(6)
	$5d_{5/2}$	11.17(7)	47.4(6)
	$6d_{5/2}$	3.65(5)	3.7(1)
	$7d_{5/2}$	2.28(3)	1.27(3)
	$5g_{7/2}$	2.73(3)	1.76(4)
	$6g_{7/2}$	2.21(2)	1.11(2)
	$5g_{9/2}$	9.64(7)	22.0(3)
	$6g_{9/2}$	7.80(6)	13.7(2)
	α_c		14.50(9)
	α_{cn}		0.24(3)
	α_{tail}		−4.83(5)
	α_{total}		−1732(41)

APPENDIX A: FARLEY AND WING'S FUNCTIONS

With the aid $|y| \gg 1$, the following expression [26]

$$F_L(y) = \frac{1}{\pi}\frac{L+1}{L(2L+1)!!(2L-1)!!} \times \int_0^\infty \left(\frac{1}{y+x}+\frac{1}{y-x}\right)\frac{x^{2L+1}}{e^x-1}dx, \quad \text{(A1)}$$

for $L = 1$, we have

$$F_1(y) = \frac{2}{3\pi}\int_0^\infty \left(\frac{1}{y+x}+\frac{1}{y-x}\right)\frac{x^3}{e^x-1}dx = \frac{2}{3\pi}\left(\frac{2}{y}\int_0^\infty \frac{x^3}{e^x-1}dx + \frac{2}{y^3}\int_0^\infty \frac{x^5}{e^x-1}dx\right). \quad \text{(A2)}$$

Further, by using the definite integral value

$$\int_0^\infty \frac{x^{2n-1}}{e^{px}-1}dx = (-1)^{n-1}\left(\frac{2\pi}{p}\right)^{2n}\frac{B_{2n}}{4n}, \quad \text{(A3)}$$

where B_{2n} is the Bernoulli number, $F_1(y)$ reduces to

$$F_1(y) = \frac{4\pi^4}{45y}. \quad \text{(A4)}$$

Similarly for $L = 2$, the above expression turns out to be

$$\begin{aligned} F_2(y) &= \frac{1}{30\pi}\int_0^\infty \left(\frac{1}{y+x}+\frac{1}{y-x}\right)\frac{x^5}{e^x-1}dx \\ &= \frac{1}{15y}\int_0^\infty \frac{x^5}{e^x-1}dx + \frac{2}{y^3}\int_0^\infty \frac{x^7}{e^x-1}dx \\ &= \frac{8\pi^5}{945y}. \end{aligned} \quad \text{(A5)}$$

APPENDIX B: SQUARE OF THE MATRIX ELEMENT

In our approach, we write

$$|\Psi_n\rangle = a_n^\dagger\Omega_c|\Phi_0\rangle + \Omega_{cn}|\Phi_v\rangle + \Omega_n|\Phi_v\rangle. \quad \text{(B1)}$$

With this expression, the square of the matrix element of any arbitrary operator O can be expressed as

$$\begin{aligned} \langle\Psi_n|O|\Psi_m\rangle^2 &= \langle\Psi_n|O|\Psi_m\rangle\langle\Psi_m|O|\Psi_n\rangle \\ &= \langle\Phi_0|\Omega_c^\dagger O\Omega_m\Omega_m^\dagger O\Omega_c|\Phi_0\rangle \\ &\quad + \langle\Phi_0|\Omega_c^\dagger O\Omega_{cm}\Omega_{cm}^\dagger O\Omega_c|\Phi_0\rangle \\ &\quad + \langle\Phi_n|\Omega_{cn}^\dagger O\Omega_c\Omega_c^\dagger O\Omega_{cn}|\Phi_n\rangle \\ &\quad + \langle\Phi_n|\Omega_n^\dagger O\Omega_c\Omega_c^\dagger O\Omega_n|\Phi_n\rangle \\ &\quad + \langle\Phi_n|\Omega_n^\dagger O\Omega_{cm}\Omega_{cm}^\dagger O\Omega_n|\Phi_n\rangle \\ &\quad + \langle\Phi_n|\Omega_n^\dagger O\Omega_m\Omega_m^\dagger O\Omega_n|\Phi_n\rangle, \end{aligned} \quad \text{(B2)}$$

where we have facilitated the generalized Wick's theorem to derive these terms and assumed all the operators are in normal order form and only the connected terms are survived. For simplicity the first two terms, the third term, and the last three terms are categorized into core (c), core-valence (cn), and valence (n) correlation contributions, respectively; i.e., in an abbreviate form it is given as

$$\langle\Psi_n|O|\Psi_m\rangle^2 = \langle\Psi_n|O|\Psi_m\rangle_c^2 + \langle\Psi_n|O|\Psi_m\rangle_{cn}^2 + \langle\Psi_n|O|\Psi_m\rangle_n^2. \quad \text{(B3)}$$

APPENDIX C: DIFFERENT FORM OF POLARIZABILITY EXPRESSION

Multipole polarizability of an atomic state $|\Psi_n\rangle$ is defined as

$$\alpha_n^{Q_L^\lambda} = C_n^{Q_L^\lambda}\sum_{m\neq n}\frac{\left|\langle\Psi_n|\left|Q_L^\lambda\right||\Psi_m\rangle\right|^2}{E_n - E_m}. \quad \text{(C1)}$$

We can rewrite the above expression as

$$\alpha_n^{Q_L^\lambda} = \frac{2}{\alpha^{2(\lambda-1)}} \sum_{m\neq n} \frac{\langle\Psi_n|Q_L^\lambda|\Psi_m\rangle\langle\Psi_m|Q_L^\lambda|\Psi_n\rangle}{E_n - E_m}$$
$$= \frac{2}{\alpha^{2(\lambda-1)}} \langle\Psi_n|Q_L^\lambda|\Psi_n^{(1)}\rangle, \quad \text{(C2)}$$

where we define

$$|\Psi_n^{(1)}\rangle = \sum_{m\neq n} |\Psi_m\rangle \frac{\langle\Psi_m|Q_L^\lambda|\Psi_n\rangle}{E_n - E_m}. \quad \text{(C3)}$$

[1] P. Gill, Metrologia **42**, S125 (2005).
[2] S. A. Diddams *et al.*, Science **293**, 825 (2001).
[3] T. Rosenband *et al.*, Science **319**, 1808 (2008).
[4] W. H. Oskay *et al.*, Phys. Rev. Lett. **97**, 020801 (2006).
[5] S. Bize *et al.*, Phys. Rev. Lett. **90**, 150802 (2003).
[6] K. Matsubara, K. Hayasaka, Y. Ling, H. Ito, S. Nagano, M. Kajita, and M. Hosokawa, Appl. Phys. Express **1**, 067011 (2008).
[7] H. S. Margolis, G. P. Barwood, G. Huang, H. A. Klein, S. N. Lea, K. Szymaniec, and P. Gill, Science **306**, 19 (2004).
[8] P. Dubé, A. A. Madej, J. E. Bernard, L. Marmet, J. S. Boulanger, and S. Cundy, Phys. Rev. Lett. **95**, 033001 (2005).
[9] C. W. Chou, D. B. Hume, J. C. J. Koelemeij, D. J. Wineland, and T. Rosenband, Phys. Rev. Lett. **104**, 070802 (2010).
[10] T. Schneider, E. Peik and Chr. Tamm, Phys. Rev. Lett. **94**, 230801 (2005).
[11] J. A. Sherman, W. Trimble, S. Metz, W. Nagourney, and N. Fortson, Digest of the LEOS Summer Topical Meetings (IEEE No. 05TH8797, 2005), e-print arXiv:physics/0504013v2.
[12] B. K. Sahoo, Phys. Rev. A **74**, 020501(R) (2006).
[13] B. K. Sahoo, B. P. Das, R. K. Chaudhuri, D. Mukherjee, R. G. E. Timmermans, and K. Jungmann, Phys. Rev. A **76**, 040504(R) (2007).
[14] O. O. Versolato, L. W. Wansbeek, K. Jungmann, R. G. E. Timmermans, L. Willmann, and H. W. Wilschut, Phys. Rev. A **83**, 043829 (2011).
[15] Th. Becker, J. v. Zanthier, A. Yu. Nevsky, Ch. Schwedes, M. N. Skvortsov, H. Walther, and E. Peik, Phys. Rev. A **63**, 051802(R) (2001).
[16] Y. H. Wang, R. Dumke, T. Liu, A. Stejskal, Y. N. Zhao, J. Zhang, Z. H. Lu, L. J. Wang, T. Becker, and H. Walther, Opt. Commun. **273**, 526 (2007).
[17] K. Hosaka, S. A. Webster, A. Stannard, B. R. Walton, H. S. Margolis, and P. Gill, Phys. Rev. A **79**, 033403 (2009).
[18] C. W. Chou, D. B. Hume, T. Rosenband, and D. J. Wineland, Science **329**, 1630 (2010).
[19] V. A. Dzuba and V. V. Flambaum, Phys. Rev. A **61**, 034502 (2000).
[20] V. V. Flambaum and A. F. Tedesco, Phys. Rev. C **73**, 055501 (2006).
[21] M. Mizushima, Phys. Rev. **133**, A414 (1964).
[22] S. H. Autler and C. H. Townes, Phys. Rev. **100**, 703 (1955).
[23] J. W. Farley and W. H. Wing, Phys. Rev. A **23**, 2397 (1981).
[24] Bindiya Arora, M. S. Safronova, and Charles W. Clark, Phys. Rev. A **76**, 052516 (2007).
[25] Dansha Jiang, Bindiya Arora, M. S. Safronova, and Charles W. Clark, J. Phys. B: At. Mol. Opt. Phys. **42**, 154020 (2009).
[26] S. G. Porsev and A. Derevianko, Phys. Rev. A **74**, 020502(R) (2006).
[27] B. K. Sahoo, R. G. E. Timmermans, B. P. Das, and D. Mukherjee, Phys. Rev. A **80**, 062506 (2009).
[28] B. K. Sahoo, B. P. Das, and D. Mukherjee, Phys. Rev. A **79**, 052511 (2009).
[29] M. Kallay, H. S. Nataraj, B. K. Sahoo, B. P. Das, and L. Visscher, Phys. Rev. A **83**, 030503 (2011).
[30] C. Champenois, M. Houssin, C. Lisowski, M. Knoop, G. Hagel, M. Vedel, and F. Vedel, Phys. Lett. A **331**, 298 (2004).
[31] Y. Huang, Q. Liu, J. Cao, B. Ou, P. Liu, H. Guan, X. Huang, and Kelin Gao, Phys. Rev. A **84**, 053841 (2011).
[32] A. A. Madej, J. E. Bernard, P. Dube, L. Marmet, and R. S. Windeler, Phys. Rev. A **70**, 012507 (2004).
[33] H. S. Margolis, G. Huang, G. P. Barwood, S. N. Lea, H. A. Klein, W. R. C. Rowley, P. Gill, and R. S. Windeler, Phys. Rev. A **67**, 032501 (2003).
[34] J. E. Bernard, A. A. Madej, L. Marmet, B. G. Whitford, K. J. Siemsen, and S. Cundy, Phys. Rev. Lett. **82**, 3228 (1999).
[35] W. R. Johnson, D. R. Plante, and J. Sapirstein, Adv. At. Mol. Opt. Phys. **35**, 255 (1995).
[36] D. Mukherjee, B. K. Sahoo, H. S. Nataraj, and B. P. Das, J. Phys. Chem. A **113**, 12549 (2009), and references therein.
[37] D. Mukherjee, R. Moitra, and A. Mukhopadhyay, Mol. Phys. **33**, 955 (1977).
[38] I. Lindgren, in *Atomic, Molecular, and Solid-State Theory, Collision Phenomena, and Computational Method*, edited by Per-Olov Lwdin and Yngve hrn (John Wiley & Sons, New York, 1978).
[39] U. Kaldor, J. Chem. Phys. **87**, 4676 (1987).
[40] R. M. Sternheimer, Phys. Rev. **96**, 951 (1954).
[41] A. Dalgarno and J. T. Lewis, Proc. R. Soc. London, Ser. A **233**, 70 (1955).
[42] Yu. Ralchenko, F.-C. Jou, D. E. Kelleher, A. E. Kramida, A. Musgrove, J. Reader, W. L. Wiese, and K. Olsen, NIST Atomic Spectra Database [Available online: http://physics.nist.gov/asd3].
[43] C. F. Roos, M. Chwalla, K. Kim, M. Riebe, and R. Blatt, Nature (London) **443**, 316 (2006).
[44] G. P. Barwood, H. S. Margolis, G. Huang, P. Gill, and H. A. Klein, Phys. Rev. Lett. **93**, 133001 (2004).
[45] B. K. Sahoo, M. R. Islam, B. P. Das, R. K. Chaudhuri, and D. Mukherjee, Phys. Rev. A **74**, 062504 (2006).
[46] B. K. Sahoo, Chem. Phys. Lett. **448**, 144 (2007).
[47] M. S. Safronova and U. I. Safronova, Phys. Rev. A **83**, 012503 (2011).